

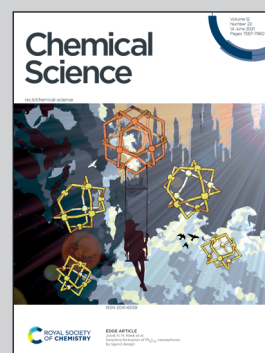


Showcasing research from Professor Nabeshima's laboratory, Faculty of Pure and Applied Sciences, University of Tsukuba, Tsukuba, Japan.

Solvent-dependent *fac/mer*-isomerization and self-assembly of triply helical complexes bearing a pivot part

An unprecedented *facial/meridional* isomerisation of a labile tris(2,2'-bipyridine) Fe^{II} complex governed by the solvent change was achieved by using tripodal ligands with a flexible linker. Furthermore, imine bond formation of the complexes with a suitable diamine quantitatively produced well-defined self-assemblies that contained only the *facial* isomer, even though a mixture of the two isomers existed in solution before the condensation reaction. Namely, the self-assembly formation effectively adjusted the geometries of the building unit that results in the suitable supramolecular structure.

As featured in:







See Tatsuya Nabeshima *et al.*, *Chem. Sci.*, 2021, **12**, 7720.

Cite this: *Chem. Sci.*, 2021, 12, 7720

All publication charges for this article have been paid for by the Royal Society of Chemistry

Solvent-dependent *fac/mer*-isomerization and self-assembly of triply helical complexes bearing a pivot part†

Takuma Morozumi,  Ryota Matsuoka,  ‡ Takashi Nakamura  and Tatsuya Nabeshima *

Tris-chelate metal complexes of unsymmetrical bidentate ligands can form two geometric stereoisomers, *facial* (*fac*) and *meridional* (*mer*) isomers. Due to the small difference in their properties, the highly-selective synthesis of one of the isomers is challenging. We now designed a series of tripodal ligands with a tris(3-(2-(methyleneoxy)ethoxy)phenyl)methane pivot. Surprisingly, the ratio of the *fac/mer* isomers of the triply helical Fe^{II} complexes significantly changed depending on the solvents. To the best of our knowledge, this is the first example of *fac/mer* isomerism of a labile tris(2,2'-bipyridine) Fe^{II} complex governed by the solvent. Furthermore, well-defined self-assemblies were quantitatively produced by imine bond formation with a suitable diamine. The supramolecular assemblies contained only the *fac* isomer even though a mixture of the two isomers existed in solution before the condensation reaction. Namely, the self-assembly formation effectively adjusted the geometries of the building unit that results in the suitable supramolecular structure.

Received 17th March 2021

Accepted 16th April 2021

DOI: 10.1039/d1sc01529j

rsc.li/chemical-science

Introduction

Tris-chelate metal complexes of unsymmetrical bidentate ligands can form two geometric stereoisomers, *facial* (*fac*) and *meridional* (*mer*) isomers. When an unsymmetrical bidentate ligand reacts with a metal ion to give the octahedral tris(ligand) complex, the statistical ratio of the *fac* and *mer* isomers is 1 : 3. The structures of the two isomers are different, but their physical and chemical properties are usually similar. Due to the small difference in their properties, the highly-selective synthesis of one of the isomers is challenging. Useful but limited strategies have been reported. The electronic and structural properties of ligands, such as the trans influence,¹ steric hindrance,² π - π interaction,³ tripodal structures,⁴ and their combination,⁵ have been successfully applied to control the isomerism. It is worth noting here that the ligands usually dominate the isomeric equilibrium. The conversion between the isomers using the same ligand is more difficult, but it leads to dynamic structural switching in response to environmental change or external stimuli.⁶⁻⁸ In supramolecular chemistry, the

fac/mer isomerism has recently attracted considerable attention to create elaborate self-assemblies consisting of metal ions and ligands. Diimine ligands such as 2,2'-bipyridine and 2-pyridylimine derivatives are widely used to construct and govern the designed structures and functions,⁹ and other bidentate ligands such as catechol derivatives are also effectively employed.¹⁰ For instance, completely different assembled structures were obtained by utilizing the *fac/mer* interconversion based on the solvent or counter ions.^{9,10}

We have studied allosteric molecular recognition by the tripodal ligands bearing three oligoether-bipyridine arms.¹¹ Recently, we reported the first example of the perfectly selective synthesis of a *meridional* triply helical complex.¹² This *meridional* complex has a unique structure in which one bipyridine unit penetrates into the cyclic cavity provided by the other two oligoether arms and the benzene pivot unit. As a result, the ion recognition ability of the tripodal molecule has been successfully suppressed. Most of the triply helical complexes reported so far are *facial* isomers,⁴ but our example demonstrated that a tripodal ligand that is appropriately designed can be utilized as a *meridional* building block. We have also reported a self-assembly system using Schiff-base formation of a triply helical *facial* complex.¹³ The triply helical building unit was exclusively obtained by the complexation of Fe²⁺ or Ru²⁺ with a tripodand in which three bipyridyl ligands are directly attached to a tris(2-methyleneoxyphenyl)methane pivot.

In this context, we envisaged that a pivot structure with the appropriate space and flexibility would result in a different ligation behavior towards a metal ion to give octahedral

Faculty of Pure and Applied Sciences and Tsukuba Research Center for Energy Materials Science (TREMS), University of Tsukuba, 1-1-1 Tennodai, Tsukuba, Ibaraki 305-8571, Japan. E-mail: nabesima@chem.tsukuba.ac.jp

† Electronic supplementary information (ESI) available: Synthetic procedures, characterization data, and X-ray crystallographic analysis. CCDC 2067281. For ESI and crystallographic data in CIF or other electronic format see DOI: 10.1039/d1sc01529j

‡ Present Address: Institute for Molecular Science, Okazaki, Aichi 444-8787, Japan.



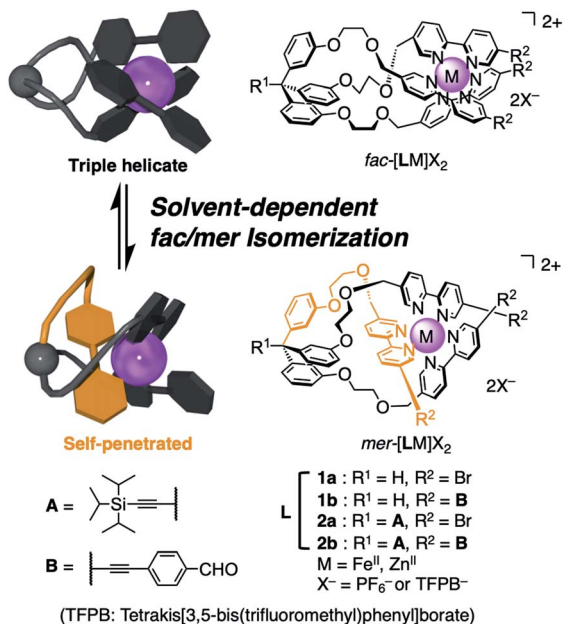


Fig. 1 Schematic representations of the interconversion between the *facial* (*fac*) and *meridional* (*mer*) isomers and chemical structures of both isomers of [LM]X₂ (L: tripodal ligands (**1a**, **1b**, **2a**, and **2b**); M: octahedral metal; X: anion).

complexes with a different *fac/mer* ratio in response to their environments. We now designed a series of tripodal ligands **L** (**1a**, **1b**, **2a**, and **2b**) with a tris(3-(2-(methyleneoxy)ethoxy)phenyl)methane pivot (Fig. 1). Surprisingly, the ratio of the *fac/mer* isomers of the triply helical Fe^{II} complexes significantly changed depending on the solvents. We found that the Hansen solubility parameters¹⁴ fit well with the *fac/mer* equilibrium ratio in different solvents. To the best of our knowledge, this is the first example of *fac/mer* isomerism of a labile tris(2,2'-bipyridine) Fe^{II} complex depending on the solvent change. Furthermore, well-defined self-assemblies were quantitatively produced by imine bond formation of [2bFe]²⁺ with a suitable diamine. The supramolecular assemblies contained only the *facial* isomer even though a mixture of the two isomers existed in solution before the condensation reaction. Namely, the self-assembly formation effectively adjusted the geometries of the building unit that results in the suitable supramolecular structure.

Results and discussion

Synthesis and characterization of tripodal ligands and their Fe^{II} complexes

Four tripodal ligands **1a**, **1b**, **2a**, and **2b** were synthesized. The common part is a tris(3-(2-(methyleneoxy)ethoxy)phenyl)methane pivot and three 2,2'-bipyridine units. The *meta*-substituted pivot instead of *ortho*-substituted one in the previous study¹³ provides more molecular freedom. Moreover, the flexible 2-(methyleneoxy)ethoxy linker also allows many conformations without steric constraints. **1a** is the simplest ligand with a methine proton at the pivot unit and a 5-bromo

group at the bipyrindyl units. **2a** and **2b** have a (triisopropylsilyl) ethynyl group (**A** in Fig. 1) at the pivot carbon to investigate the structural effect and use for possible structural extension in future studies. In **1b** and **2b**, three 4-formylphenylethynyl groups (**B** in Fig. 1) were introduced, which are employed for the self-assembly of the triply helical complexes *via* imine bond formation.

The tripodal ligand **2b** possessing both units **A** and **B** is explained in detail below. **2b** was synthesized by the reaction of a tris(3-hydroxyphenyl)methane derivative ("a pivot part") and a mesylated 2-(5'-bromo-2,2'-bipyridyl)ethanol derivative ("a coordination part"), followed by the Sonogashira cross-coupling reaction with 4-ethynylbenzaldehyde to introduce unit **B**. [2bFe](PF₆)₂ was then obtained by the complexation of this ligand with Fe(BF₄)₂ and the exchange of the counter anion to PF₆⁻. The synthetic procedures for **2b** and [2bFe](PF₆)₂, as well as those for **1a**, **1b**, **2a** and their Fe^{II} complexes, are described in the ESI (¹H NMR spectra and ESI-MS are shown in Fig. S1–S18, S28–S35 and S41–S45†).

The ¹H NMR spectrum of [2bFe](PF₆)₂ in CD₃CN indicated that this complex is a mixture of the *facial* and *meridional* isomers (Fig. 2a and S41†). Focusing on the signals of the

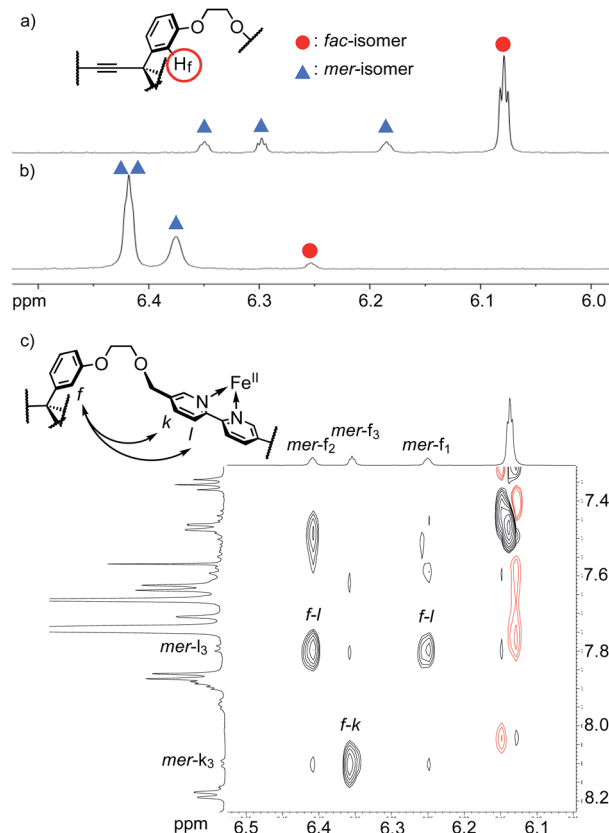


Fig. 2 (a and b) ¹H NMR spectra of [2bFe](PF₆)₂ (600 MHz, 5.9–6.5 ppm). (a) CD₃CN. (b) CDCl₃. (c) ¹H–¹H ROESY spectrum of [2bFe](TFPB)₂. See Fig. S47† for the detailed assignment of the signals. The characteristic ROE correlations supporting the structure of *mer*-[2bFe](TFPB)₂ are highlighted (signals of the *mer*-isomer are numbered for each tripodal arm).



proton *f* (2 position of the benzene ring of the pivot, see Fig. S41† for the assignment of the other ^1H NMR signals), there are one large signal at 6.08 ppm (denoted with a red circle in Fig. 2) and three small signals with an equal intensity at 6.18, 6.30, and 6.35 ppm (denoted with blue triangles in Fig. 2). The signal at 6.08 ppm was assigned to the *facial* isomer and the three signals at 6.18, 6.30, and 6.35 ppm were assigned to the *meridional* isomer based on symmetry: The *facial* isomer has C_3 symmetry but the *meridional* isomer does not. It is considered that the appropriate length and flexibility of the ethylene glycol chains enabled the formation of these two isomers. The *fac/mer* ratio calculated from the integral values of the proton signals was 71 : 29. Considering the statistical ratio of *fac/mer* = 25 : 75, the *facial* isomer of $[\mathbf{2bFe}](\text{PF}_6)_2$ was favored in CD_3CN .

Solvent dependence on *fac/mer* isomerism of $[\mathbf{2bFe}]^{2+}$

When the solvent of the sample of $[\mathbf{2bFe}](\text{PF}_6)_2$ was changed to CDCl_3 from CD_3CN , only a small signal was found at 6.25 ppm, and two large signals were observed at 6.38 and 6.42 ppm with the ratio of 2 : 1 (Fig. 2b and S77†). This result showed that the equilibrium significantly shifted toward the *meridional* isomer in CDCl_3 . The sample solution was heated at 50 °C for 12 hours and cooled to r.t. to reach the *fac/mer* equilibrium of 4 : 96. To further investigate this interesting phenomenon, the *fac/mer* ratios of $[\mathbf{2bFe}]^{2+}$ (as well as the Gibbs free energy ΔG) were determined by ^1H NMR measurements in various deuterated solvents. Due to the poor solubility of $[\mathbf{2bFe}](\text{PF}_6)_2$ in low-polar solvents, $[\mathbf{2bFe}](\text{TFPB})_2$ (TFPB: tetrakis[3,5-bis(trifluoromethyl)phenyl]borate) was synthesized (Fig. S46–S51†), which exhibited a good solubility in a wide range of solvents (CD_3CN , CDCl_3 , CD_3OD , acetone- d_6 , CD_3NO_2 , $\text{CD}_3\text{CO}_2\text{D}$, CD_2Cl_2 , THF- d_8 , DMF- d_7 , dioxane- d_8 , *o*-dichlorobenzene- d_4 : *o*-DCB- d_4 , tetrachloroethane- d_2 : TCE- d_2). The ^1H - ^1H ROESY spectrum of $[\mathbf{2bFe}](\text{TFPB})_2$ showed cross peaks between the proton *f* (pivot unit) and the protons *k,l* (3,4 positions of bipyridyl) of the *meridional* isomer (Fig. 2c and S47†). This suggested that the *meridional* isomer had a self-penetrated structure in which one bipyridine unit was surrounded by the other two bipyridines and the triphenylmethane of the pivot unit.

The *fac/mer* ratios of $[\mathbf{2bFe}](\text{TFPB})_2$ changed from 10 : 90 to 71 : 29 depending on the solvents (Table 1 and Fig. S66†). The *meridional* isomers are favored in halogenated solvents (TCE- d_2 (10 : 90), CDCl_3 (10 : 90)), but other than this point, it seems difficult to find a good factor to fit this trend at first glance. DMF- d_7 (32 : 68), which is generally regarded as a highly polar solvent (ϵ (dielectric constant): 36.7), and CD_2Cl_2 (40 : 60), which is generally regarded as a less polar solvent (ϵ : 8.9), gave similar isomer ratios. Thus, this solvent dependence was assumed to be a complex phenomenon involving factors other than polarity.

For some solvents, the changes in enthalpy ΔH and entropy ΔS upon the conversion from the *mer* isomer to the *fac* isomer were determined by the van't Hoff analysis of variable-temperature NMR measurements of $[\mathbf{2bFe}](\text{TFPB})_2$ (Table 1 and Fig. S67–S71†). As a result, both ΔH and ΔS were negative in all the investigated solvents. Thus, the *facial* isomer is

Table 1 The ratios of the *fac/mer* isomers of $[\mathbf{2bFe}](\text{TFPB})_2$ and thermodynamic parameters for the isomerization from *mer* to *fac* in various solvents (298 K)

Solvent	<i>fac/mer</i>	ΔG (kJ mol $^{-1}$)	ΔH^a (kJ mol $^{-1}$)	$T\Delta S^a$ (kJ mol $^{-1}$)
TCE- d_2	10 : 90	5.5	—	—
CDCl_3	10 : 90	5.5	−9.2	−14
<i>o</i> -DCB- d_4	13 : 87	4.8	—	—
Dioxane- d_8	20 : 80	3.4	—	—
DMF- d_7	32 : 68	1.8	−4.2	−6.0
THF- d_8	34 : 66	1.7	−11	−13
CD_2Cl_2	40 : 60	1.1	—	—
$\text{CD}_3\text{CO}_2\text{D}$	53 : 47	−0.31	—	—
CD_3NO_2	57 : 43	−0.70	—	—
CD_3OD	64 : 36	−1.5	—	—
Acetone- d_6	69 : 31	−2.0	−22	−20
CD_3CN	71 : 29	−2.2	−12	−10

^a Determined by van't Hoff analysis of VT NMR measurements.

enthalpically favorable and the *meridional* isomer is entropically favorable. It appears that the changes in the *fac/mer* ratio (*i.e.*, ΔG) were not correlated very well with ΔH or ΔS , which suggested that this isomerization cannot be explained by a simple factor. One of the causes would be the degree of formation of ion pairs, but the details could not be explained (Table S2, Fig. S72 and S73†).

Solvent dependence of the other complexes

To investigate the effect of substituents (units **A** and **B** in Fig. 1) of the tripodand on the solvent dependence, $[\mathbf{1aFe}](\text{TFPB})_2$, $[\mathbf{1bFe}](\text{TFPB})_2$, and $[\mathbf{2aFe}](\text{TFPB})_2$ were synthesized (Fig. S19–S27 and S36–S40†), and their *fac/mer* ratios were determined in CD_3CN and CDCl_3 (Table 2). As a result, the *fac/mer* ratios of all the complexes depended on the solvents in a similar manner with $[\mathbf{2bFe}](\text{TFPB})_2$, that is, *facial* isomers were favored in CD_3CN , while *meridional* isomers increased in CDCl_3 (Fig. S74–S77†). Furthermore, it was confirmed that the *fac/mer* ratio of a Zn^{II} complex, $[\mathbf{2bZn}](\text{TFPB})_2$ (Fig. S52–S56†), showed the same tendency (90 : 10 in CD_3CN , 67 : 33 in $\text{CD}_3\text{CN}/\text{CDCl}_3 = 1 : 4$, Fig. S78†). For comparison, the monobipyridine ligand **3b** and its tris(ligand) complex $[(\mathbf{3b})_3\text{Fe}](\text{TFPB})_2$ were synthesized (Fig. 3, spectral data of characterization are shown in Fig. S57–S65†). As a result, the *fac/mer* ratio of $[(\mathbf{3b})_3\text{Fe}](\text{TFPB})_2$ showed no solvent dependence (22 : 78 in CD_3CN , 21 : 79 in CDCl_3 , Fig. S79†). Thus, the tris(3-(2-methoxyethoxy)phenyl)methane unit of $[\mathbf{2bFe}](\text{TFPB})_2$ plays a key role in the solvent-dependent *fac/mer* isomerism.

Correlation with Hansen solubility parameters

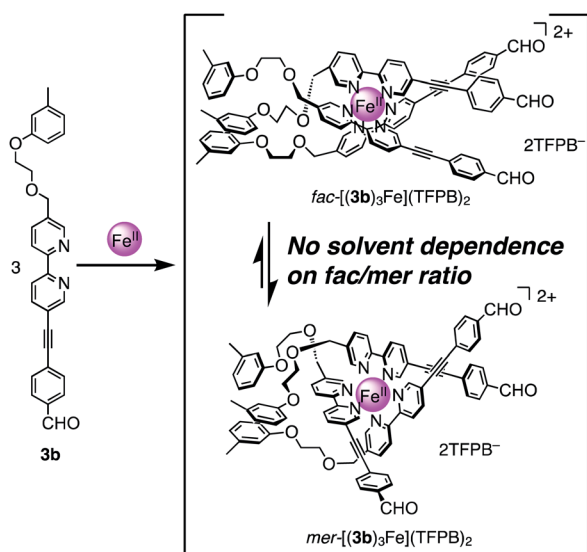
In order to clarify the factor involved in the solvent dependency of the *fac/mer* isomerism of $[\mathbf{2bFe}](\text{TFPB})_2$, the correlations between the ΔG of the *fac/mer* isomerization and the major solvent parameters were evaluated in terms of the correlation coefficient *R* by a linear regression analysis (Fig. 4, Tables S1 and S3†). The correlations of ΔG with the dielectric constant ϵ and dipole moment μ , both of which are typical solvent



Table 2 Solvent effects on the *fac/mer*-isomerization equilibrium of various complexes^a

Complex	Difference from [2bFe](TFPB) ₂	<i>fac/mer</i> in CD ₃ CN	<i>fac/mer</i> in CD ₃ CN/CDCl ₃ = 1/4	<i>fac/mer</i> in CDCl ₃
[2bFe](TFPB) ₂	—	71 : 29	39 : 61	10 : 90
[1aFe](TFPB) ₂	No group A, B	83 : 17	—	64 : 36
[1bFe](TFPB) ₂	No group A	76 : 24	—	22 : 78
[2aFe](TFPB) ₂	No group B	75 : 25	—	13 : 87
[2bFe](PF ₆) ₂	PF ₆ ⁻	71 : 29	—	4 : 96
[2bZn](TFPB) ₂	Zn ^{II}	90 : 10	67 : 33	—
[(3b) ₃ Fe](TFPB) ₂	Without pivot	22 : 78 ^b	—	21 : 79 ^b

^a The *fac/mer* ratios were calculated from the signals of the proton *f* (2 position of the benzene ring of the pivot) (see Fig. 2). ^b Calculated from the signals of the formyl proton *q* (see Fig. S61).

Fig. 3 Chemical structures of both isomers of [(3b)₃Fe](TFPB)₂.

parameters, were less than 0.7, indicating no strong correlation (Fig. 4a and b). The donor number DN and the acceptor number AN¹⁵ had very low correlation coefficients ($|R| < 0.3$), which suggested that coordination or basicity of the solvents did not affect this *fac/mer* isomerism (Fig. 4c and d). Meanwhile, the molar volume V_m showed a good correlation ($R = 0.83$) (Fig. 4e).

Among the tested parameters, we found that the Hansen solubility parameters (HSPs)¹⁴ showed the strongest correlations. HSPs are the parameters used for the prediction of solubility, and represented by three independent values; *i.e.*, the dispersion term (δ_d), the dipole interaction term (δ_p), and the hydrogen bonding term (δ_h). HSPs have long been used in the fields of polymers and coatings in which understanding of the interaction between solvents and solutes is essential, and been also recently applied to many fields such as drugs¹⁶ and supramolecular gels.¹⁷ We found that the ΔG of *fac/mer* isomerization is strongly correlated ($R = 0.87$) with δ_d , the dispersion term of HSPs (Fig. 4f). The correlations with the other two terms (δ_p and δ_h) were weak to moderate (Fig. 4g and h), but the multiple correlation coefficient with the combination of δ_d and δ_p was as high as 0.91 (Fig. 4i and Table S3[†]). Thus, this result

suggested that a difference in the solvation by dispersion forces between the *fac/mer* isomers plays a key role in the solvent-dependent isomerization equilibrium.

Structural comparison of *fac/mer* isomers

In efforts to obtain single crystals of the complexes, we have succeeded in the structural analysis of *fac*-[1aFe](PF₆)₂ by X-ray diffraction measurements (Fig. 5a–c and S80[†]). As suggested by the ¹H NMR measurements, the *facial* isomer has a pseudo C_3 symmetry in the crystal. The methine proton of the triaryl-methane pivot unit was directed outward. For comparison, the structure of *mer*-[1aFe](PF₆)₂ obtained using DFT calculations is shown in Fig. 5d–f. Considering the result of linear regression analyses and the difference in molecular structures, one possible explanation for the solvent-dependent isomerization is the degree of exposure to the solvent. The [Fe(bpy)₃]²⁺ of the *facial* isomer is exposed to the solvent. Meanwhile, the self-penetrated bipyridyl unit of *mer*-[Fe(bpy)₃]²⁺ is surrounded by the triaryl-methane pivot and the ethylene glycol chains. As shown in Fig. 4, the correlation efficient between the *fac/mer* ratio and δ_d ($R = 0.87$) indicates that the solvation by the dispersion force is more favored for the *mer* isomer than the *fac* isomer. Meanwhile, the correlation efficient with δ_p ($R = -0.73$) indicates that the solvation by the dipole interaction is more favored for the *fac* isomer than the *mer* isomer. The structural difference of the *fac/mer* isomers, *i.e.*, exposure of [Fe(bpy)₃]²⁺ unit to the solvent, seems to be a factor to explain this dependency of the *fac/mer* ratio on the HSPs. Other possible factors to be included in the causes of the solvent-dependence are the inclusion of a solvent molecule in the *fac*-[Fe(bpy)₃]²⁺ (an acetone molecule was found in the cavity, Fig. S80[†] (X-ray crystallography)) and the formation of an ion pair (Table S2, Fig. S72 and S73 (¹H DOSY)[†]).

Reversibility in *fac/mer* conversion and self-assembly with diamines

The solvent-dependent *fac/mer* isomerization of [2bFe](TFPB)₂ was found to be reversible (Fig. S82[†]). The sample was dried *in vacuo*, alternatively redissolved in CD₃CN and CDCl₃, and ¹H NMR was performed. The interchange between the *fac/mer* ratios in the solvents can be repeated at least five times (Fig. S81[†]).



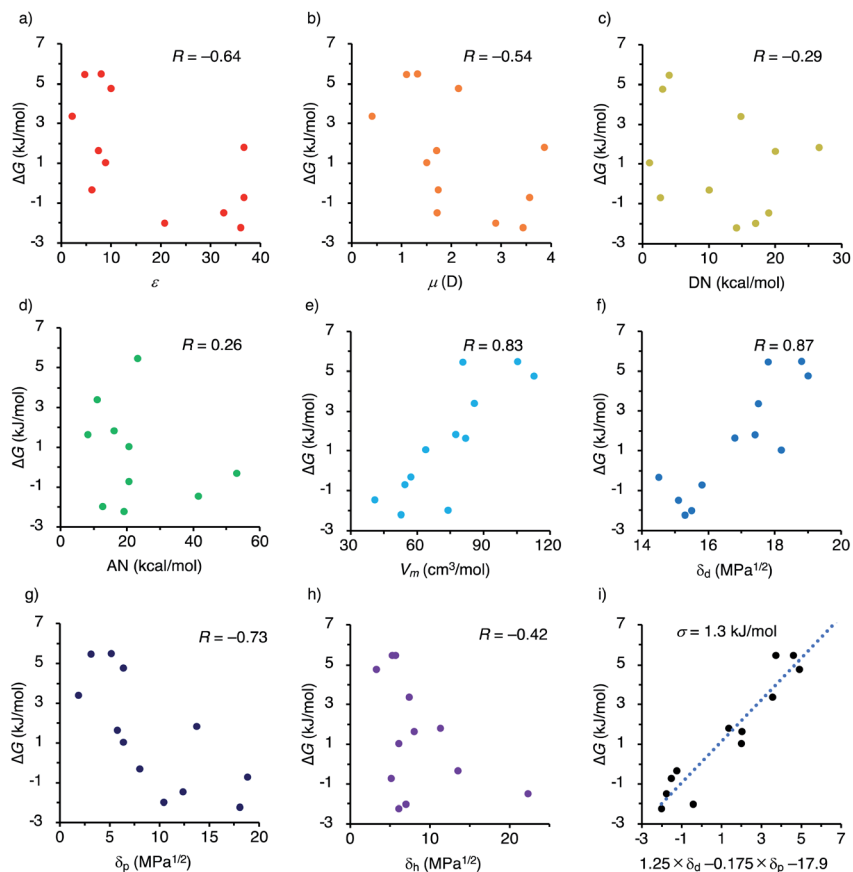


Fig. 4 ΔG (*mer* to *fac*) plotted versus various solvent parameters and their correlation coefficient. (a) Dielectric constant ϵ ,^{15a} (b) dipole moment μ (D),^{15a} (c) donor number DN (kcal mol^{-1}),^{15a,b} (d) acceptor number AN (kcal mol^{-1}),^{15a} (e) molar volume V_m ($\text{cm}^3 \text{mol}^{-1}$),¹⁴ (f–h) the Hansen solubility parameters,¹⁴ (f) dispersion term δ_d ($\text{MPa}^{1/2}$),¹⁴ (g) dipole interaction term δ_p ($\text{MPa}^{1/2}$),¹⁴ (h) hydrogen bonding term δ_n ($\text{MPa}^{1/2}$),¹⁴ and (i) a prediction formula using δ_d and δ_p as explanatory variables.

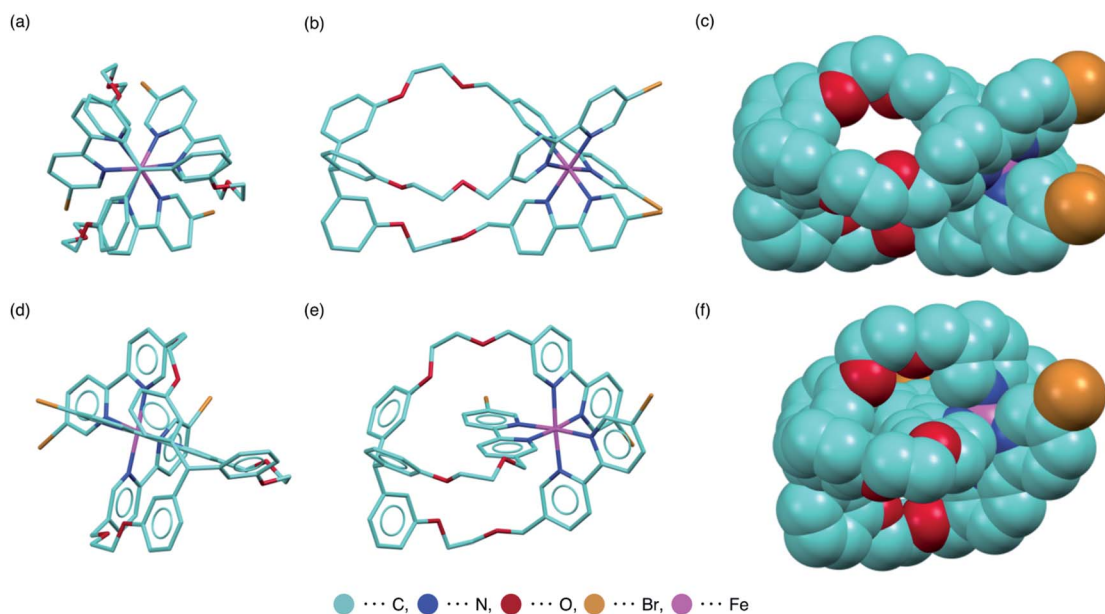


Fig. 5 Comparison of the two isomers of $[\mathbf{1aFe}]^{2+}$ (hydrogen atoms are omitted. (a, b, d and e); stick model, (c and f); space-fill model). (a–c) A molecular structure of *fac*- $[\mathbf{1aFe}]^{2+}$ determined by X-ray diffraction analysis. (a) Top view. (b and c) Side view. (d–f) A structure of *mer*- $[\mathbf{1aFe}]^{2+}$ obtained by DFT calculation (B3LYP/6-31G*). (d) Top view. (e and f) Side view.



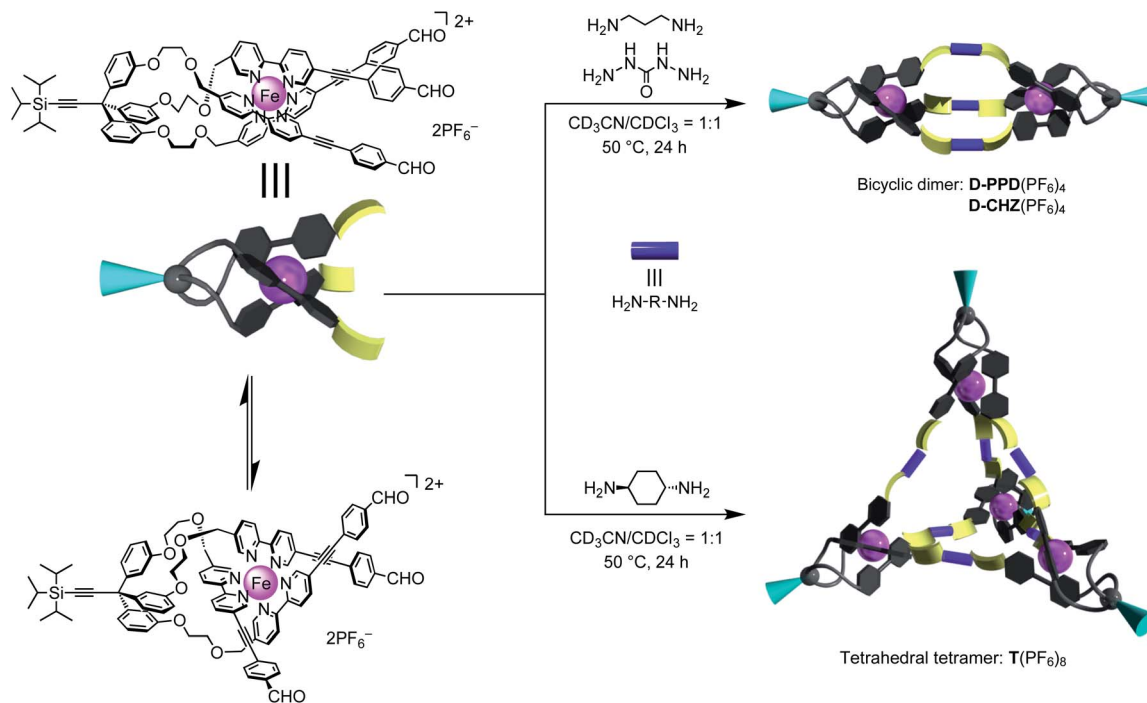


Fig. 6 Bicyclic dimer D-PPD^{4+} and D-CHZ^{4+} , and tetrahedral tetramer T^{8+} , which are constructed by the imine bond formation of $[\text{2bFe}]^{2+}$ existing as a *fac/mer* isomeric mixture.

As a further application of $[\text{2bFe}]^{2+}$ bearing three terminal formyl groups, the self-assembly *via* the Schiff-base formation was investigated (Fig. 6). $[\text{2bFe}](\text{PF}_6)_2$ was treated with 1.5 equiv. of 1,3-propanediamine in $\text{CD}_3\text{CN}/\text{CDCl}_3 = 1/1$. ^1H NMR spectrum after the reaction revealed the disappearance of the signals of the formyl group at 10.00 ppm, and the appearance of a singlet of an imine bond at 8.31 ppm (Fig. S83 \dagger), which confirmed quantitative imine bond formation. The obtained product has C_3 symmetry on the NMR time scale. The ESI-TOF mass measurements gave signals assigned to chemical species formed from two $[\text{2bFe}]^{2+}$ and three diamines (Fig. S86 \dagger). The NMR and MS data indicated that the obtained product was the bicyclic dimer D-PPD^{4+} composed of the *facial* isomer (Fig. 6, spectral data of characterization are shown in Fig. S83–S86 \dagger). Thus, *fac/mer* equilibrium of $[\text{2bFe}]^{2+}$ was completely shifted to the *fac*-isomer during the process of Schiff-base formation. When the carbohydrazide was used as a linker molecule, the ^1H NMR and ESI-MS indicated that a similar bicyclic dimer, D-CHZ^{4+} , was constructed (Fig. S88 and S89 \dagger). On the other hand, when *trans*-1,4-cyclohexanediamine reacted under the same condition, the ESI-TOF MS indicated that the species formed from four $[\text{2bFe}]^{2+}$ and six diamines (Fig. S93 \dagger). The ^1H NMR spectrum supported the quantitative formation of an imine bond and the high symmetry of the obtained product (Fig. S90 \dagger). These results suggested the formation of the tetrahedral tetramer T^{8+} composed of the *facial* isomer (Fig. 6, spectral data of characterization are shown in Fig. S90–S93 \dagger). The hydrodynamic radii evaluated from the DOSY spectra increased in the order of the mononuclear complex $[\text{2bFe}](\text{PF}_6)_2$, bicyclic dimer $\text{D-PPD}(\text{PF}_6)_4$, and tetrahedral tetramer $\text{T}(\text{PF}_6)_8$ (12, 17, and 25 Å, respectively, Table S4, Fig. S87 and S94 \dagger), which

supported the formation of the assemblies. The discrete self-assemblies depending on the components can be applied to the dynamic combinatorial library or adaptive chemistry.¹⁸

Conclusions

We have synthesized novel tripodal ligands **L** (**1a**, **1b**, **2a**, and **2b**), and revealed that the *fac/mer* ratios of their octahedral complexes $[\text{LM}]\text{X}_2$ ($\text{M} = \text{Fe}^{\text{II}}$ or Zn^{II}) ($\text{X} = \text{PF}_6$ or TFPB) largely depend on the solvents. This solvent-dependent isomerization occurs regardless of the counter anion, the metal center, and the substituents on the bipyridine and the pivot unit. It was found that the dispersion term δ_d of the Hansen solubility parameters (HSPs) showed a good correlation with ΔG of the *fac/mer* isomerization. Considering the good fitting result of this study, it would be interesting to apply HSPs to other supramolecular systems in which solvation plays an important role. Moreover, when using $[\text{2bFe}]^{2+}$ as a component for the self-assembly *via* imine bond formation, discrete dimeric and tetrameric structures were obtained accompanied by the conversion from the *fac/mer* isomeric mixture to the pure *facial* isomer. This structure with an appropriate pivot part with flexible chains is demonstrated to be a good building block for supramolecular systems that change their structures in response to the environmental change.

Author contributions

R. M. and T. Nabeshima conceived the project. T. M., R. M. and T. Nabeshima designed the experiments. T. M. carried out the



experimental work. T. M. and R. M. performed X-ray measurements and analysis. All the authors analysed the data, prepared the manuscript, and contributed to the writing of the paper.

Conflicts of interest

There are no conflicts to declare.

Acknowledgements

This research was supported by JSPS KAKENHI (Grant Numbers JP18H01959, JP19K15579, JP19K15578, JP19H04559, and JP20H05202), the Mazda Foundation, Inamori Foundation, Ogasawara Foundation, and Iketani Science and Technology Foundation.

References

- (a) A. Grabulosa, M. Beley and P. C. Gros, *Eur. J. Inorg. Chem.*, 2008, 1747–1751; (b) L. Aboshyan-Sorgho, T. Lathion, L. Guénée, C. Besnard and C. Piguet, *Inorg. Chem.*, 2014, **53**, 13093–13104.
- (a) M. A. Case, M. R. Ghadiri, M. W. Mutz and G. L. McLendon, *Chirality*, 1998, **10**, 35–40; (b) N. C. Fletcher, M. Nieuwenhuyzen and S. Rainey, *J. Chem. Soc., Dalton Trans.*, 2001, 2641–2648; (c) M. Gochin, V. Khorosheva and M. A. Case, *J. Am. Chem. Soc.*, 2002, **124**, 11018–11028; (d) M. Kyakuno, S. Oishi and H. Ishida, *Chem. Lett.*, 2005, **34**, 1554–1555.
- S. E. Howson, L. E. N. Allan, N. P. Chmel, G. J. Clarkson, R. van Gorkum and P. Scott, *Chem. Commun.*, 2009, 1727–1729.
- (a) H. Weizman, J. Libman and A. Shanzer, *J. Am. Chem. Soc.*, 1998, **120**, 2188–2189; (b) N. C. Fletcher, M. Nieuwenhuyzen, R. Prabakaran and A. Wilson, *Chem. Commun.*, 2002, 1188–1189; (c) N. C. Fletcher, R. T. Brown and A. P. Doherty, *Inorg. Chem.*, 2006, **45**, 6132–6134; (d) B. Brisig, E. C. Constable and C. E. Housecroft, *New J. Chem.*, 2007, **31**, 1437–1447.
- (a) S. E. Howson, L. E. N. Allan, N. P. Chmel, G. J. Clarkson, R. J. Deeth, A. D. Faulkner, D. H. Simpson and P. Scott, *Dalton Trans.*, 2011, **40**, 10416–10433; (b) M. Kieffer, B. S. Pilgrim, T. K. Ronson, D. A. Roberts, M. Aleksanyan and J. R. Nitschke, *J. Am. Chem. Soc.*, 2016, **138**, 6813–6821; (c) T. Nakamura, S. Yonemura, S. Akatsuka and T. Nabeshima, *Angew. Chem., Int. Ed.*, 2021, **60**, 3080–3086.
- (a) S. Sakai, Y. Shigemasa and T. Sasaki, *Tetrahedron Lett.*, 1997, **38**, 8145–8148; (b) S. Sakai, Y. Shigemasa and T. Sasaki, *Bull. Chem. Soc. Jpn.*, 1999, **72**, 1313–1319.
- N. Ousaka, Y. Takeyama and E. Yashima, *Chem.–Eur. J.*, 2013, **19**, 4680–4685.
- V. Cámara, N. Barquero, D. Bautista, J. Gil-Rubio and J. Vicente, *Chem.–Eur. J.*, 2015, **21**, 1992–2002.
- (a) S. L. Dabb and N. C. Fletcher, *Dalton Trans.*, 2015, **44**, 4406–4422; (b) I. A. Riddell, M. M. J. Smulders, J. K. Clegg, Y. R. Hristova, B. Breiner, J. D. Thoburn and J. R. Nitschke, *Nat. Chem.*, 2012, **4**, 751–756; (c) I. A. Riddell, Y. R. Hristova, J. K. Clegg, C. S. Wood, B. Breiner and J. R. Nitschke, *J. Am. Chem. Soc.*, 2013, **135**, 2723–2733; (d) S. Zarra, J. K. Clegg and J. R. Nitschke, *Angew. Chem., Int. Ed.*, 2013, **52**, 4837–4840; (e) R. A. Bilbeisi, T. K. Ronson and J. R. Nitschke, *Angew. Chem., Int. Ed.*, 2013, **52**, 9027–9030; (f) I. A. Riddell, T. K. Ronson, J. K. Clegg, C. S. Wood, R. A. Bilbeisi and J. R. Nitschke, *J. Am. Chem. Soc.*, 2014, **136**, 9491–9498; (g) I. A. Riddell, T. K. Ronson and J. R. Nitschke, *Chem. Sci.*, 2015, **6**, 3533–3537.
- (a) M. Albrecht, X. Chen and D. Van Craen, *Chem.–Eur. J.*, 2019, **25**, 4265–4273; (b) X. Chen, C. Mevissen, S. Huda, C. Göb, I. M. Oppel and M. Albrecht, *Angew. Chem., Int. Ed.*, 2019, **58**, 12879–12882.
- (a) T. Nabeshima, *Bull. Chem. Soc. Jpn.*, 2010, **83**, 969–991; (b) T. Nabeshima, Y. Yoshihira, T. Saiki, S. Akine and E. Horn, *J. Am. Chem. Soc.*, 2003, **125**, 28–29; (c) T. Nabeshima, Y. Tanaka, T. Saiki, S. Akine, C. Ikeda and S. Sato, *Tetrahedron Lett.*, 2006, **47**, 3541–3544; (d) T. Nabeshima, S. Masubuchi, N. Taguchi, S. Akine, T. Saiki and S. Sato, *Tetrahedron Lett.*, 2007, **48**, 1595–1598.
- H. Morita, S. Akine, T. Nakamura and T. Nabeshima, *Chem. Commun.*, 2021, **57**, 2124–2127.
- T. Nakamura, H. Kimura, T. Okuhara, M. Yamamura and T. Nabeshima, *J. Am. Chem. Soc.*, 2016, **138**, 794–797.
- C. M. Hansen, *Hansen Solubility Parameters: A User's Handbook*, CRC Press LLC, Boca Raton, Florida, USA, 2nd edn, 2007.
- (a) U. Mayer, V. Gutmann and W. Gerger, *Monatsh. Chem.*, 1975, **106**, 1235–1257; (b) F. Cataldo, *Eur. Chem. Bull.*, 2015, **4**, 92–97.
- (a) X. Zhang, Q. Yin, X. Li, M. Zhang, J. Huang, C. Wang, Z. Zhang, Y. Huang, M. Guo and Y. Li, *J. Mol. Liq.*, 2017, **237**, 46–53; (b) A. M. Navarro, B. García, F. J. Hoyuelos, I. A. Peñacoba and J. M. Leal, *Fluid Phase Equilib.*, 2016, **429**, 127–136.
- (a) J. Gao, S. Wu and M. A. Rogers, *J. Mater. Chem.*, 2012, **22**, 12651–12658; (b) M. Zhang, S. Selvakumar, X. Zhang, M. P. Sibi and R. G. Weiss, *Chem.–Eur. J.*, 2015, **21**, 8530–8543; (c) T. Wang, X. Yu, Y. Li, J. Ren and X. Zhen, *ACS Appl. Mater. Interfaces*, 2017, **9**, 13666–13675.
- J.-M. Lehn, *Chem. Soc. Rev.*, 2007, **36**, 151–160.

